

# A quantum-mechanical treatment of phonon scattering in carbon nanotube transistors

Jing Guo<sup>a)</sup>

Department of Electrical and Computer Engineering, University of Florida, Gainesville, Florida 32611

(Received 12 May 2005; accepted 15 August 2005; published online 27 September 2005)

Phonon scattering in carbon nanotube field-effect transistors (CNTFETs) is treated using the nonequilibrium Green's function formalism with the self-consistent Born approximation. The treatment simultaneously captures the essential physics of phonon scattering and important quantum effects. For a one-dimensional channel, it is computationally as efficient as and physically more rigorous than the so-called "Büttiker probe" approach [Phys. Rev. Lett. **57**, 1761 (1986)], which has been widely used in mesoscopic physics. The non-self-consistent simulation results confirm that the short mean-free-path optical phonon (OP) scattering, though expected to dominate even in a short channel CNTFET, essentially has no *direct* effect on the dc on current under modest gate biases. The self-consistent simulation results indicate that OP scattering, however, can have an *indirect* effect on the on current through self-consistent electrostatics. Using a high- $\kappa$  gate insulator suppresses the indirect effect and leads to a dc on current closer to the ballistic limit. The indirect effect in a CNT Schottky barrier FET can be more important than that in a metal-oxide semiconductor FET. © 2005 American Institute of Physics. [DOI: 10.1063/1.2060942]

## I. INTRODUCTION

Carbon nanotubes (CNTs) have been extensively explored for nanoelectronic applications due to their excellent electrical properties.<sup>1</sup> Scattering plays an important role on carrier transport and  $I$ - $V$  characteristics of CNTs.<sup>2-4</sup> It has been demonstrated that under low biases, the dominant scattering mechanism in a high-quality CNT is the near-elastic acoustic phonon (AP) scattering with a mean free path (mfp) of  $\sim 1 \mu\text{m}$ .<sup>2</sup> Due to the long mfp, near-ballistic transport can be readily achieved for CNTs with submicron-meter lengths.<sup>5</sup> Under high biases, the most important scattering mechanism is the short-mfp (of  $\sim 10$  nm) optical phonon (OP) scattering. Because a channel length of  $\sim 10$  nm or above is preferred for controlling the short-channel effects and preventing the source-drain tunneling,<sup>6</sup> OP scattering is expected to dominate even in a short-channel CNT field-effect transistor (FET). As the channel length of the CNTFETs is being aggressively scaled below 100 nm for potential nanoelectronic device applications,<sup>7,8</sup> it is important to clearly understand the role of phonon scattering in short-channel CNTFETs. A recent work using semiclassical simulations showed that OP scattering has a very small direct effect on the dc (on current) under modest gate biases.<sup>9</sup>

In this work, a quantum treatment of phonon scattering in CNTFETs using the nonequilibrium Green's function (NEGF) formalism with the self-consistent Born approximation<sup>10</sup> is presented. For a CNTFET with a one-dimensional channel, the approach is physically much more rigorous than and computationally as efficient as a phenomenological treatment of scattering using the Büttiker probe approach,<sup>11</sup> which has been widely used in mesoscopic physics. The direct and indirect effects of phonon scattering are

examined using non-self-consistent and self-consistent simulations, respectively, for a CNT Schottky barrier (SB) FET.<sup>12</sup> The non-self-consistent simulation results confirm that OP scattering has a very small direct effect on the dc (on current). The self-consistent simulation results indicate that OP scattering, however, can have an *indirect* effect through self-consistent electrostatics. The indirect effect in a CNT SBFET can be more important than that in a metal-oxide semiconductor (MOS) FET.<sup>13</sup>

## II. THEORY

### A. Modeled device parameters

A high-performance CNTFET with a 8 nm  $\text{HfO}_2$  top gate insulator, a 50 nm channel, and good metal/CNT contacts have been recently demonstrated.<sup>7</sup> The modeled CNTFET (as shown in Fig. 1) is similar to the CNTFET as reported in Ref. 7. The intrinsic (22, 0) zigzag CNT channel has a channel length of  $L_{\text{ch}}=50$  nm, and a diameter of  $d_{\text{CNT}}\approx 1.7$  nm, which results in a band gap of  $E_g\approx 0.49$  eV. Because the conduction and valence bands of CNTs are symmetric, we modeled the  $n$ -type conduction for convenience. The thickness of the source and drain metal contacts is 7 nm, and the metal Fermi level aligns with the first conduction subband of the CNT at the metal/CNT interface. The  $\text{HfO}_2$

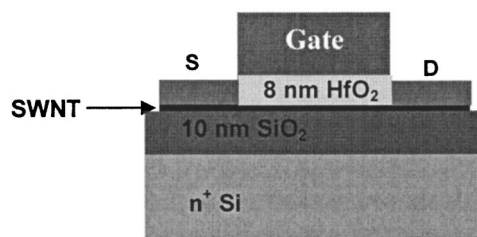


FIG. 1. The modeled CNTFET with a 50-nm-long intrinsic channel.

<sup>a)</sup>Electronic mail: guo@ufl.edu

top gate insulator is 8 nm thick with a dielectric constant of  $\kappa \approx 20$ . The  $\text{SiO}_2$  bottom insulator has a thickness of 10 nm and a dielectric constant of 3.9. The simulations were performed at the room temperature,  $T=300$  K. The work-function difference between the  $n^+$  substrate and the intrinsic CNT channel is  $-0.6$  eV, and that between the top gate electrode and the CNT is zero.

## B. Ballistic transport

The quantum treatment of phonon scattering is based on our previous work on the quantum simulation of ballistic transport in CNTFETs, which is summarized as follows.<sup>13</sup> The quantum transport equation was solved using the NEGF formalism at the ballistic limit,<sup>10</sup> which is equivalent to the open-boundary Schrödinger equation. A simple atomistic basis set with one  $p_z$  orbital per carbon atom was used in a real-space approach. The real-space approach is computationally expensive, but significant computational savings can be achieved by using a mode space approach. By performing a basis transform in the circumferential direction of the tube (which transforms the real-space lattice to plane waves satisfying periodic boundary conditions), the mode space approach decouples the two-dimensional lattice in the real space to  $n$  one-dimensional lattices in the mode space for a  $(n,0)$  zigzag CNT. Only one or a few lowest modes contribute to electrical conduction and need to be treated, and the computational cost is significantly reduced.<sup>13</sup> The mode space approach is valid when the potential variation around the tube is smaller than the spacing between the neighboring subbands. (For the modeled CNTFET, the spacing between the first and second subbands is  $\sim 0.25$  eV.)

A phenomenological treatment of the metal/CNT contacts, which has been validated by experiments,<sup>7</sup> was used.<sup>13</sup> Each semiconducting mode in the channel is coupled to the metallic mode in the metal contact, with two input parameters. The first parameter is the metal/CNT work-function difference, which determines how the subbands in the channel align with the metal contact Fermi level. The second parameter is the coupling strength between the semiconducting mode in the channel and the metallic mode in the contact, which determines the density of metal-induced gap states (MIGSs) at the interface. The treatment is at the same level as the model described by Leonard and Tersoff.<sup>14</sup> The metal-induced interface charges can produce a potential barrier near the junction, but due to the low dimensionality of the interface charges, the barrier decays rapidly with distance and does not result in Fermi-level pinning.<sup>14</sup>

A three-dimensional (3D) Poisson equation was self-consistently solved with the quantum transport equation using the method of moments.<sup>15</sup> The 3D geometry of the metal contacts was simulated in the electrostatic calculations. The iteration between the NEGF transport equation and the 3D Poisson equation continued until self-consistency was achieved. The source-drain current was finally computed using the self-consistent subband profile.<sup>13</sup>

## C. Phonon scattering in CNTs

Two phonon scattering mechanisms were identified to be important in CNTs.<sup>2-4</sup> Under low biases, near-elastic AP scattering dominates. The long mfp of AP scattering leads to near-ballistic transport in submicron tubes. Under high biases, optical phonons (with small wave vector  $\mathbf{k} \sim 0$ ) and the zone-boundary phonons (with large  $\mathbf{k}$  near the Brillouin-zone boundary) with energies between 160 and 200 meV dominate, and result in optical-intravalley scattering and optical-intervalley scattering, respectively.<sup>4,16,17</sup> OP scattering (including both intravalley and intervalley scatterings) has a much shorter mfp than AP scattering.<sup>2</sup>

The mfps of phonon scattering can be obtained by two approaches. In the first approach, the mfps are computed from the deformation potential using Fermi's golden rule.<sup>4,16,17</sup> In the second approach, the mfps are obtained by fitting the experimentally measured  $I$ - $V$  characteristics.<sup>2-4</sup> Previous studies on metallic tubes showed that although the mfps of AP scattering obtained by the first and second approaches are similar, the OP scattering mfp obtained by the first approach is several times longer than that obtained by the second approach.<sup>2,4</sup> Future work is needed to understand this discrepancy. In this study, we used the mfps obtained by fitting. Varying the mfps to the values computed from the deformation potential<sup>16</sup> does not change the qualitative results of the work.

The scattering rate in a semiconducting CNT is strongly energy dependent due to its energy-dependent density of states (DOS). At high energies, the value approaches that of a metallic tube because the  $E$ - $k$  of a semiconducting band approaches that of a metallic band. The following expression was used to describe the scattering rate in the CNT channel:

$$\frac{1}{\tau(E)} = \frac{v_F}{\lambda_{\text{AP}}^{\text{high}}} \frac{D(E)}{D_0} + \frac{v_F}{\lambda_{\text{OP}}^{\text{high}}} \frac{D(E - \hbar\omega_{\text{OP}})}{D_0}, \quad (1)$$

where  $v_F \approx 1.0 \times 10^8$  cm/s is the Fermi velocity, and  $\lambda_{\text{AP}}^{\text{high}} = 1.0 \mu\text{m}$  and  $\lambda_{\text{OP}}^{\text{high}} = 10$  nm are the backscattering mfps for AP scattering and OP scattering in a semiconducting CNT at high energies, respectively, which approach the value in metallic tubes.<sup>2</sup> AP scattering is treated as an elastic-scattering mechanism. Optical and zone-boundary phonons with an energy in the range between 160 and 200 meV scatter electrons,<sup>16,18</sup> and an average OP energy of  $\hbar\omega_{\text{OP}} = 180$  meV is used. Only phonon emission is treated because the phonon energy  $\hbar\omega_{\text{OP}} \gg k_B T$  at room temperature and the number of optical phonons at thermal equilibrium  $N_\omega \approx 0$ . (No hot phonon effect is observed in a CNTFET with a non-suspended channel for the drain bias  $V_D < 1$  V.<sup>19</sup>)  $D(E)$  is the energy-dependent DOS in the semiconducting CNT,

$$D(E) \approx D_0 \sum_\nu \frac{E + \Delta_\nu}{\sqrt{(E + \Delta_\nu)^2 - \Delta_\nu^2}} \Theta(E + \Delta_\nu - \Delta_\nu), \quad (2)$$

where  $\Delta_\nu$  is the half band gap for the  $\nu$ th subband, and  $\Theta(x)$  is the unitary step function. The energy reference point  $E = 0$  is at the bottom of the first conduction subband. Figure 2 plots the scattering rate as a function of the energy for a CNT with a diameter of  $d_{\text{CNT}} \approx 1.7$  nm.

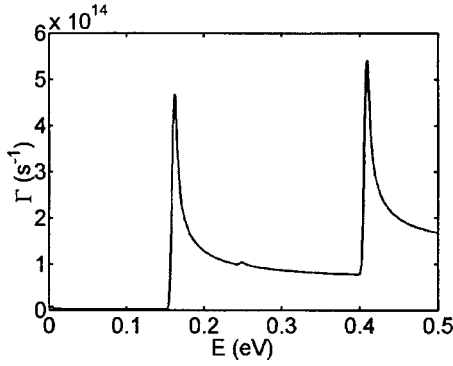


FIG. 2. The scattering rate vs energy. The energy zero is set at the bottom of the first conduction subband. Intersubband scattering is included.

### D. A NEGF treatment of phonon scattering in CNTFETs

Phonon scattering in the CNTFET is treated using the NEGF formalism with the self-consistent Born approximation.<sup>10,20</sup> For a one-dimensional channel, it is computationally as efficient as and physically more rigorous than the so-called “Büttiker probe” approach,<sup>11</sup> which has been extensively used in mesoscopic physics. Figure 3 shows the quantities used in the NEGF simulation. The channel is coupled to the subspaces with one more or one less phonon by phonon scattering. The treatment relates the in-scattering and out-scattering self-energies,  $\Sigma^{\text{in}}$  and  $\Sigma^{\text{out}}$ , to the electron and hole correlations  $G_{\nu}^n$  and  $G_{\nu}^p$  through the following relations:

$$\begin{aligned} \Sigma^{\text{in}}(E) = & |U_{\text{AP}}|^2 [I \otimes \sum_{\nu} G_{\nu}^n(E)] \\ & + |U_{\text{OP}}|^2 [I \otimes \sum_{\nu} G_{\nu}^n(E + \hbar\omega_{\text{OP}})], \end{aligned} \quad (3a)$$

$$\begin{aligned} \Sigma^{\text{out}}(E) = & |U_{\text{AP}}|^2 [I \otimes \sum_{\nu} G_{\nu}^p(E)] \\ & + |U_{\text{OP}}|^2 [I \otimes \sum_{\nu} G_{\nu}^p(E - \hbar\omega_{\text{OP}})], \end{aligned} \quad (3b)$$

where  $\nu$  is the subband index,  $\hbar\omega_{\text{OP}}$  is the OP energy,  $I$  is the identity matrix,  $\otimes$  is the element-by-element matrix multiplication, and  $|U_{\text{AP}}|^2$  and  $|U_{\text{OP}}|^2$  are the perturbation potential squares of the AP scattering and the OP scattering, respec-

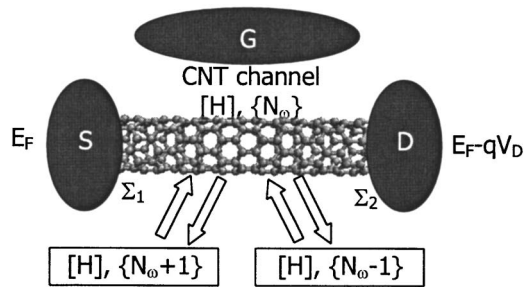


FIG. 3. The NEGF treatment of phonon scattering in a CNTFET using the self-consistent Born approximation. The CNT channel is coupled to the source (drain) contact with a self energy of  $\Sigma_1$  ( $\Sigma_2$ ). The channel has a Hamiltonian matrix ( $H$ ), and is coupled to the subspaces with one more or one less phonon,  $N_{\omega} \pm 1$ .

tively. For a zigzag CNT, they relate to the backscattering mfps by using Fermi’s golden rule,

$$|U_{\text{AP/OP}}|^2 = \frac{4(\hbar v_F)^2}{3a_{\text{cc}}\lambda_{\text{AP/OP}}^{\text{high}}}, \quad (3c)$$

where  $a_{\text{cc}}$  is the C–C bonding distance.

The broadening matrix of phonon scattering is

$$\Gamma_{\text{SCA}}(E) = \Sigma^{\text{in}}(E) + \Sigma^{\text{out}}(E), \quad (4)$$

and the self-energy matrix of phonon scattering is

$$\Sigma_{\text{SCA}}(E) \approx -\frac{i}{2}\Gamma_{\text{SCA}}(E). \quad (5)$$

The retarded Green’s function for the  $\nu$ th subband of the CNT channel is

$$G_{\nu}^r(E) = [EI - H - \Sigma_{1\nu}(E) - \Sigma_{2\nu}(E) - \Sigma_{\text{SCA}}(E)]^{-1}, \quad (6)$$

where  $H$  is the channel Hamiltonian matrix, and  $\Sigma_{1\nu/2\nu}$  is the self-energy matrix of the source/drain contact. The electron and hole correlation of the  $\nu$ th subband can be computed as

$$G_{\nu}^n(E) = G_{\nu}^r[\Gamma_{1\nu}f_s(E) + \Gamma_{2\nu}f_D(E) + \Sigma^{\text{in}}]G_{\nu}^{r+}, \quad (7a)$$

$$G_{\nu}^p = G_{\nu}^r[\Gamma_{1\nu}(1 - f_s) + \Gamma_{2\nu}(1 - f_D) + \Sigma^{\text{out}}]G_{\nu}^{r+}, \quad (7b)$$

where  $f_{S/D}(E)$  is the source/drain Fermi distribution function, and  $\Gamma_{1\nu/2\nu} = i(\Sigma_{1\nu/2\nu} - \Sigma_{1\nu/2\nu}^+)$  is the broadening matrix of the source/drain contact. The coupled quantum transport equations [Eqs. (3)–(7)] were iteratively solved until convergence was achieved.

In a non-self-consistent simulation, the potential profile was an input for the quantum transport equations [Eqs. (3)–(7)]. In a self-consistent simulation, the quantum transport equations were solved self-consistently with the Poisson equation. After self-consistency was achieved, the source and drain currents were computed as

$$I_S = \frac{4e}{h} \sum_{\nu} \int_{-\infty}^{+\infty} dE \text{Tr}(\Gamma_{1\nu}f_s A_{\nu} - \Gamma_{1\nu}G_{\nu}^n), \quad (8a)$$

$$I_D = \frac{4e}{h} \sum_{\nu} \int_{-\infty}^{+\infty} dE \text{Tr}(\Gamma_{2\nu}G_{\nu}^n - \Gamma_{2\nu}f_D A_{\nu}), \quad (8b)$$

where  $A_{\nu} = G_{\nu}^n + G_{\nu}^p$  is the spectrum function of the  $\nu$ th subband.

### III. SIMULATION RESULTS

The quantum simulations are used to examine the effect of phonon scattering on the dc (on current) of the CNTFET as shown in Fig. 1. We first self-consistently compute the band profile and the on current  $I_b$  at the ballistic limit (with  $\lambda_{\text{AP}}^{\text{high}} = \lambda_{\text{OP}}^{\text{high}} \rightarrow +\infty$ ). The solid lines in Figs. 4 and 5 show the first subband profile at the ballistic limit for the on state ( $V_D = V_G = 0.4$  V). The small potential barrier at the source/CNT interface is produced by the low-dimensional interface charges induced by the MIGS. The computed ballistic on current is  $I_b \approx 4.7 \mu\text{A}$ . In order to explore the direct effect of phonon scattering, we perform non-self-consistent simulations in the presence of only AP scattering (as shown in Fig.

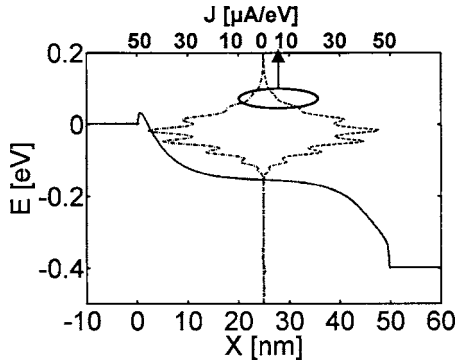


FIG. 4. The non-self-consistently computed source current spectrum (the dashed line) and the drain current spectrum (the dash-dot line) in the presence of only AP scattering. The first subband profile is shown by the solid line.

4) and in the presence of both AP and OP scatterings (as shown in Fig. 5) using the ballistic subband profile as an input. The current in the presence of phonon scattering,  $I_{nsc}$ , is computed by solving Eqs. (3)–(8). The ballistic figure of merit ( $I_{nsc}/I_b$ ) is evaluated.

In the presence of only AP scattering ( $\lambda_{AP}^{high} = 1.0 \mu\text{m}$  and  $\lambda_{OP}^{high} \rightarrow +\infty$ ), the on current  $I_{nsc}^{AP} \approx 4.4 \mu\text{A}$  is about 94% of the ballistic on current. AP scattering has a small effect on the source-drain current due to its long mfp. The dashed (dash-dot) line in Fig. 4 shows the source (drain) current spectrum versus the energy in the presence of only AP scattering. No energy relaxation occurs because AP scattering is elastic, and the source and drain current spectra are equal. Rapid oscillations due to quantum interference are observed in the simulated current spectra. Because AP scattering is weak and in the channel is short, carrier transport in the channel is near coherent. Electron waves reflected by the metal/CNT interfere with each other as in a Fabry-Perot resonator,<sup>21</sup> which results in oscillations in the current spectra.

Figure 5 shows the non-self-consistent simulation results in the presence of both AP scattering ( $\lambda_{AP}^{high} = 1.0 \mu\text{m}$ ) and OP scattering ( $\lambda_{OP}^{high} = 10 \text{nm}$ ). The dashed (dash-dot) line shows the source (drain) current spectrum. In contrast with the results in Fig. 4, energy relaxation is clearly observed in Fig. 5. When electrons travel through the channel, emitting one or a

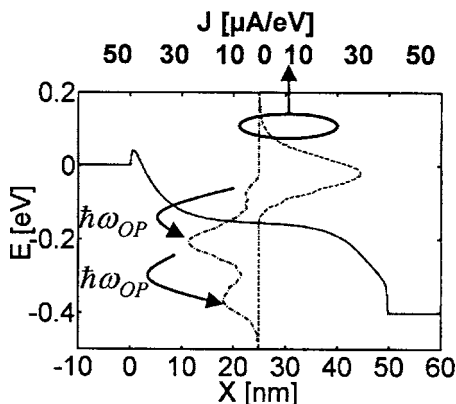


FIG. 5. The non-self-consistently computed source current spectrum (the dashed line) and the drain current spectrum (the dash-dot line) in the presence of both AP and OP scatterings. The first subband profile is shown by the solid line.

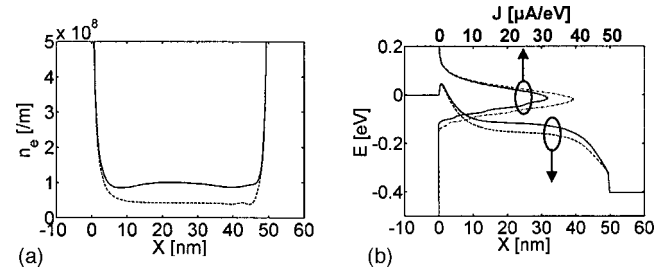


FIG. 6. The self-consistent simulation results for the CNTFET as shown in Fig. 1. (a) The electron densities and (b) the first conduction subband profiles at the ballistic limit (the dashed line) in the presence of AP and OP scatterings (the solid lines). The top axis of (b) shows the current spectra computed in the presence of scattering. The dash-dot line is computed using the dashed band profile, and the solid line is computed using the solid band profile.

few OPs results in the peak values on the drain current spectrum below the peak of the source current spectrum (as shown in Fig. 5). Because the OP scattering mfp is several times shorter than the channel length, carrier transport in the channel is noncoherent and the rapid oscillations in the current spectra (as shown in Fig. 4) are not observed.

Although OP scattering has a significant effect on the current spectra, the quantum simulations confirm that its direct effect on the dc is very small, as described in a recent study using semiclassical simulations.<sup>9</sup> The simulated on current in the presence of both AP and OP scatterings,  $I_{nsc} \approx 4.4 \mu\text{A}$ , is approximately the same as that in the presence of only AP scattering. The OP scattering essentially has no direct effect on the on current for the following reason. After emitting an OP, whose energy is much larger in a CNT than in common semiconductors, a backscattered electron encounters a much higher and thicker Schottky barrier at the source end, and can hardly return back to the source.<sup>9</sup> The OP scattering, though occurs even in a short-channel CNTFET, has a very small direct effect on the current under modest gate biases. The above results cannot be obtained by the phenomenological Büttiker probe approach<sup>11</sup> because it does not model the phonon energy of each scattering mechanism.

We next perform the self-consistent simulations by solving the quantum transport equations self-consistently with the Poisson equation in the presence of phonon scattering. Figure 6(a) shows that phonon scattering results in a larger electron density in the channel region. The reason is that phonon scattering leads to random walks of carriers and lowers the average carrier velocity. The charge density in the channel must increase to maintain a similar source-drain current. Due to a self-consistent potential produced by the larger electron density, the band profile in the channel region moves up as shown in Fig. 6(b), which reduces the source-drain current. As shown by the current spectra plotted in Fig. 6(b), compared with the non-self-consistently computed current spectrum (the dash-dot line), the self-consistently computed current spectrum (the solid line) delivers a smaller current density in a narrower energy window. The self-consistently computed on current is  $I_{sc} \approx 3.7 \mu\text{A}$ , and is about 80% of the ballistic on current. Although the OP scattering essentially has no *direct* effect on the source-drain dc, it lowers the ballistic figure of merit from 94% to 80% due to the *indirect*

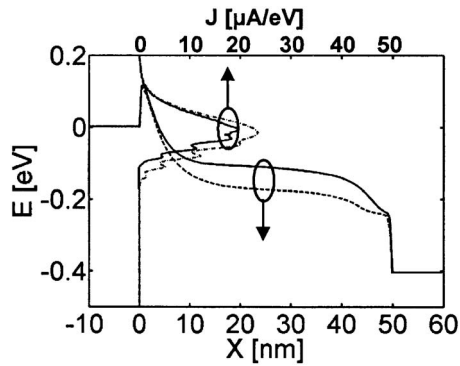


FIG. 7. The self-consistent simulation results for the CNTFET as shown in Fig. 1 but with a  $\text{SiO}_2$  top gate insulator. The bottom axis shows the first conduction subband profiles at the ballistic limit (the dashed line) and in the presence of AP and OP scatterings (the solid lines). The top axis shows the current spectra computed in the presence scattering. The dash-dot line is computed using the dashed band profile, and the solid line is computed using the solid band profile.

effect of phonon scattering through self-consistent electrostatics.

Using a high- $\kappa$  gate insulator suppresses the indirect effect by reducing the self-consistent potential. For comparison, we simulated a CNTFET as shown in Fig. 1 with a  $\text{SiO}_2$  top gate insulator, instead of a  $\text{HfO}_2$  gate insulator. The dashed line in Fig. 7 shows the self-consistent subband profile at the ballistic limit, with a ballistic on current of  $I'_b \approx 3.00 \mu\text{A}$ . Compared with the high- $\kappa$  insulator case, the ballistic on current decreases because the same amount of interface is less efficiently screened by the  $\text{SiO}_2$  gate insulator, which results in a thicker Schottky barrier at  $E_F=0$ .<sup>22</sup> The dash-dot line shows the non-self-consistently computed current spectrum in the presence of AP and OP scatterings (the dash-dot line) using the ballistic subband profile, which corresponds to an on current of  $\sim 2.87 \mu\text{A}$ , about 95% of  $I'_b \approx 3.00 \mu\text{A}$ . The non-self-consistent calculation confirms the small direct effect of phonon scattering. The solid lines plot the self-consistently computed subband profile (at the bottom axis) and the current spectrum (at the top axis) in the presence of AP and OP scatterings. The comparison of Figs. 6(b) and 7 indicates that the self-consistent potential due to the increased charge density in the channel is larger for a  $\text{SiO}_2$  gate insulator, because its gate insulator capacitance is smaller. The self-consistently computed on current in the presence of scattering is  $I'_{sc} \approx 2.1 \mu\text{A}$ , and the ballistic figure of merit is about 70%. The indirect effect of phonon scattering through self-consistent electrostatics lowers the ballistic figure of merit from 95% to 70%, which is more severe than it does for the CNTFET with a high- $\kappa$  gate insulator. The application of a high- $\kappa$  insulator not only increases the ballistic current of a CNTFET, but also facilitates the transistor to deliver an on current closer to its ballistic limit by suppressing the indirect effect of phonon scattering.

The indirect effect in an unconventional SBFET behaves in both similar and different ways as in a conventional MOSFET.<sup>20</sup> Figures 8(a) and 8(b) sketch the subband profile and an OP emission event under a modest gate bias in a CNT SBFET and in a CNT MOSFET,<sup>23</sup> respectively. For the CNT SBFET, the current is controlled by quantum tunneling

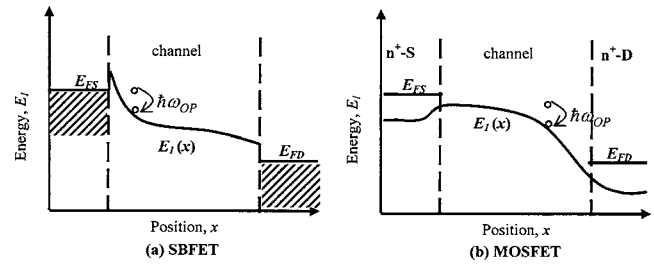


FIG. 8. The schematic sketch of the first subband profile and an OP emission event for (a) a SBFET and (b) a MOSFET with a similar channel length and on current under a modest gate bias.

through the Schottky barrier at the source end of the channel. For the CNT MOSFET, the current is controlled by thermionic emission over the top of the barrier at the beginning of the channel.<sup>24</sup> For both transistors, OP scattering can result in pile up of charge in the channel, and affects the potential profile near the source through a two-dimensional electrostatic effect.<sup>6</sup> The indirect effect in the CNT SBFET, however, is expected to be more severe than that in the CNT MOSFET. As shown in Fig. 8, the potential profile at the beginning of the channel in the CNT SBFET varies much more rapidly than in the CNT MOSFET for a similar on current. As a result, the source-injected electrons in the CNT SBFET can gain enough energy and emit an optical phonon within a distance much shorter than that in the CNT MOSFET. The pile up of charge in a CNT SBFET occurs closer to the beginning of the channel, and has a larger effect on the potential profile at the beginning of the channel, which controls the source-drain current. The indirect effect, therefore, is expected to be more important in the CNT SBFET.

The simulation results presented above are for a CNTFET with a 50 nm channel length at a gate voltage of 0.4 V, and we also examined the indirect effect of phonon scattering at different channel lengths and gate voltages. For a short channel CNT SBFET ( $I_{ch} < 100 \text{ nm}$ ), because the indirect effect affects the on current by modifying the Schottky barrier at the source end of the channel, the qualitative conclusions remain the same for different channel lengths as long as the channel length is larger than the OP scattering mfp ( $\sim 10 \text{ nm}$ ). When the gate voltage is varied, we find that the indirect effect is more important at higher gate voltages when a larger percentage of source-injected carriers encounter OP scattering and the charge density in the channel is larger.

#### IV. SUMMARY

We presented a self-consistent quantum treatment for phonon scattering in CNTFETs using the NEGF formalism with the self-consistent Born approximation. The essential physics of phonon scattering and important quantum effects are simultaneously captured. The approach is physically more rigorous than the Büttiker probe approach because it physically treats each scattering mechanism with its phonon energy, which plays an important role on determining the effect of scattering. For a one-dimensional channel, it is computationally as efficient as the Büttiker probe approach.

We show that although its *direct* effect is small due to large OP energies, the short-mfp OP scattering can affect the source drain dc *indirectly* through the self-consistent electrostatics. The application of a high- $\kappa$  gate insulator not only increases the ballistic current of a CNTFET, but also facilitates the transistor to deliver a source-drain dc closer to its ballistic limit by suppressing the indirect effect of the OP scattering. The indirect effect in a CNT SBFET is expected to be more important than that in a CNT MOSFET.

## ACKNOWLEDGMENTS

The author would like to thank Professor M. Lundstrom, Professor S. Datta, S. Koswatta of Purdue University, and Dr. M. Paulsson of Danish Technical University for helpful discussions. The computational facility was made possible from the NSF Grant No. EIA-0224442, IBM SUR grants and gifts, and a DURIP grant from the Army Research Office.

- <sup>1</sup>P. Avouris, J. Appenzeller, R. Martel, and S. J. Wind, Proc. IEEE **91**, 1772 (2003); P. L. McEuen, M. S. Fuhrer, and H. K. Park, IEEE Trans. Nanotechnol. **1**, 78 (2002).  
<sup>2</sup>Z. Yao, C. L. Kane, and C. Dekker, Phys. Rev. Lett. **84**, 2941 (2000).  
<sup>3</sup>A. Javey, J. Guo, M. Paulsson, Q. Wang, D. Mann, M. Lundstrom, and H. Dai, Phys. Rev. Lett. **92**, 106804 (2004).  
<sup>4</sup>J. Y. Park, Nano Lett. **4**, 517 (2004).  
<sup>5</sup>A. Javey, J. Guo, Q. Wang, and H. Dai, Nature (London) **424**, 654 (2003); S. J. Wind, J. Appenzeller, and P. Avouris, Phys. Rev. Lett. **91**, 058301 (2003).  
<sup>6</sup>Y. Taur and T. Ning, *Fundamentals of Modern VLSI Devices* (Cambridge University Press, London, UK, 1998).

- <sup>7</sup>A. Javey, J. Guo, D. B. Farmer, Q. Wang, E. Yenilmez, R. G. Gordon, M. Lundstrom, and H. Dai, Nano Lett. **4**, 1319 (2004).  
<sup>8</sup>R. V. Seidel *et al.*, Nano Lett. **5**, 147 (2005).  
<sup>9</sup>J. Guo and M. Lundstrom, Appl. Phys. Lett. **86**, 193103 (2005).  
<sup>10</sup>S. Datta, *Electronic Transport in Mesoscopic Systems* (Cambridge University Press, Cambridge, UK, 1995).  
<sup>11</sup>M. Buttiker, Phys. Rev. Lett. **57**, 1761 (1986); R. Venugopal, M. Paulsson, S. Goasguen, S. Datta, and H. Lundstrom, J. Appl. Phys. **93**, 5613 (2003).  
<sup>12</sup>J. Appenzeller, J. Knoch, V. Derycke, R. Martel, S. Wind, and Ph. Avouris, Phys. Rev. Lett. **89**, 126801 (2002); S. Heinze, J. Tersoff, R. Martel, V. Derycke, J. Appenzeller, and Ph. Avouris, Phys. Rev. Lett. **89**, 106801 (2002).  
<sup>13</sup>J. Guo, S. Datta, M. Lundstrom, and M. P. Anantram, Int. J. Multiscale Comp. Eng. **2**, 257 (2004).  
<sup>14</sup>F. Leonard and J. Tersoff, Phys. Rev. Lett. **84**, 4693 (2000).  
<sup>15</sup>S. Ramo, J. R. Whinnery, and T. Van Duzer, *Fields and Waves in Communication Electronics*, 3rd ed. (Wiley, New York, NY, 1993).  
<sup>16</sup>V. Perebeinos, J. Tersoff, and P. Avouris, Phys. Rev. Lett. **94**, 027402 (2005).  
<sup>17</sup>G. D. Mahan, Phys. Rev. B **68**, 125409 (2003).  
<sup>18</sup>G. Pennington and N. Goldsman, Phys. Rev. B **68**, 045426 (2003).  
<sup>19</sup>E. Pop, D. Mann, J. Cao, Q. Wang, K. Goodson, and H. Dai, e-print cond-mat/0506122.  
<sup>20</sup>A. Svizhenko and M. P. Anantram, IEEE Trans. Electron Devices **50**, 1459 (2003).  
<sup>21</sup>W. J. Liang, M. Bockrath, D. Bozovic, J. H. Hafner, M. Tinkham, and H. Park, Nature (London) **411**, 665 (2001).  
<sup>22</sup>J. Guo, S. Datta, and M. Lundstrom, IEEE Trans. Electron Devices **51**, 172 (2004).  
<sup>23</sup>J. Chen, C. Klinke, A. Afzali, and Ph. Avouris, Appl. Phys. Lett. **86**, 123108 (2005).  
<sup>24</sup>M. Lundstrom and Z. B. Ren, IEEE Trans. Electron Devices **49**, 133 (2002).